Angle-resolved photoelectron spectra of $YBa_2Cu_3O_{7-\delta}$ and their line-shape analysis

N. Schroeder, R. Böttner, S. Ratz, E. Dietz, and U. Gerhardt
Physikalisches Institut der Universität, Robert-Mayer-Strasse 2-4, D-6000 Frankfurt am Main, Germany

Th. Wolf
Kernforschungszentrum Karlsruhe, Institut für Technische Physik, P.O. Box 3640, D-7500 Karlsruhe, Germany
(Received 9 September 1991; revised manuscript received 27 July 1992)

We measure the high-resolution photoelectron spectra of twinned $YBa_2Cu_3O_{7-\delta}$ single crystals cleaved at about 10 K in ultrahigh vacuum perpendicular to the c axis for various angles of detection along the Γ-$X(Y)$ azimuth. The spectra in general and the 1-eV peak in particular strongly depend on the cleavage plane investigated, with correlated changes observable in the low-energy-electron-diffraction pattern: For the surface showing a distorted $c(2\times2)$ superlattice the 1-eV surface-state peak is missing; the electronic structure at this surface seems to show the smallest deviations from that of the bulk. The spectral features measured at this surface can be assigned to at least four different branches of the calculated energy bands. A quadratic dependence of the linewidth on the binding energy, a symmetrical line shape of the spectra, and the identification of a clear Fermi edge above T_c also support a Fermi-liquid description. At temperatures well below T_c the spectra of this surface show some indications of BCS-type modifications close to E_F, while no hint for them could be detected for the numerous cleavage planes showing the 1-eV peak.

I. INTRODUCTION

In spite of the rapid evolution in the field of the high-temperature superconductors (HTSC), no commonly accepted theory describing the state of these materials above and below T_c exists.[1] The band-structure calculations using the local-density approximation (LDA) provide an important starting point, but these calculations neglect the electron correlations believed to be important. This problem can be investigated by angle-resolved photoelectron spectroscopy (ARPES) since it allows one to determine the band structure of a crystal and to extract information about the electron correlations as well. The merits of this method can best be elucidated by referring to the model system Cu and Ni,[2–5] with the $3d$ shell completely and only partly filled, respectively. The electron correlations can thus be neglected for Cu but play an important role in Ni.

Except for the position of the Fermi energy E_F (2 eV above the top of the $3d$ bands for Cu and slightly below it for Ni) and the exchange splitting Δ_x (zero for paramagnetic Cu and between 0.2 and 0.3 eV for ferromagnetic Ni), the calculated energy bands are very similar for both materials. A pronounced similarity is also found for most ARPES features of Cu and Ni. In particular, the strong dependence of the line intensity on the angle of observation, the orientation of the polarization vector $\mathbf{A}$ of the incident radiation, and the photon energy are just the same in Cu and Ni, taking the differences in E_F and Δ_x into account. These intensity variations are caused by the dependence of the transition probability on $\mathbf{A}$ and $\mathbf{k}$, and also by the variation in the number of states contributing to a particular line. For that reason only about 30% of the existing initial states can be identified for a particular geometry of detection.

On the other hand, compared to Cu, in Ni the width of the ARPES lines increases much more rapidly with the binding energy of the initial state, the experimentally determined band is narrower than the calculated one, and a satellite structure below the $3d$ band which is not given by the LDA calculation shows up in ARPES. These three phenomena are caused by the large electron correlations in Ni. Guided by this comparison, we thus first analyze the ARPES of Y-Ba-Cu-O on the basis of the LDA bands. Afterwards, we try to identify the three phenomena mentioned above in order to assess the importance of the electron correlations.

ARPES is a surface sensitive method, since the escape depth of the photoelectrons is only a few angstroms. Thus adsorbed layers or major changes in the electron distribution or the atomic position at the surface will produce spectra no longer representative of the bulk. In the case of Y-Ba-Cu-O it is particularly difficult to prepare the required "ideal" surfaces which approach the bulk electronic and structural properties. The first photoelectron spectra for this class of HTSC showed no Fermi edge, probably because the spectra were taken at semiconducting or reconstructed surfaces, but they induced far-reaching theoretical speculations nevertheless. Cleavage planes of the $Bi_2Sr_2CaCu_2O_8$ (Bi2:2:1:2) HTSC between the weakly bonded Bi—O double layers are much more stable, the ARPES taken at these surfaces not only show a clear Fermi energy but also allow the identification of CuO- and BiO-derived bands crossing E_F (Refs. 6,7) as well as other band-structure features at higher binding energies.[8] In addition, the spectra indicate the opening of the superconducting gap below T_c as described by the BCS theory.[9–12] In succeeding papers ARPES of Y-Ba-Cu-O cleaved at low temperatures showed a sharp Fermi edge and a band dispersing away

from it roughly as predicted by the LDA calculations.[13–16] Our paper, which is complementary to a recent ARPES study[13] at $h\nu=21.22$ eV, focuses on the low photon energies and addresses the problem of decomposing the spectra into the individual lines as a precondition to determine the dependence of the linewidth on the binding energy and to enable the comparison with the LDA bands.

The spectra presented here are obtained from numerous cleavage planes generated *in situ* at temperatures of 20 K and below. Two of these are unique in that they do *not* show the strong 1-eV peak which we obtain for the vast majority of surfaces generated in the same way, but a pronounced structure near E_F as strong or even stronger than that observed for the spectra showing the 1-eV peak. There are two indications that this 1-eV peak originates from a surface state: the characteristic modifications in the electronic structure induced by each of the six possible cleavage planes were calculated recently within the LDA, assuming no change in the atomic positions.[17] According to this calculation, the 1-eV peak which is prominent in all the spectra reported in two recent publications[13,16] is characteristic of breaking the long Cu(2)—O(4) bond, i.e., of the surfaces designated $CuO_2(b)$ and $BaO(b)$ in Fig. 1. The sensitivity of this 1 eV feature to the adsorption of reactive gases (to be discussed in detail later on) which also identifies it as a surface state is clearly compatible with this interpretation. The spectra lacking the 1-eV peak might therefore originate from a different cleavage plane, yielding ARPES more characteristic of the bulk, as we have already suggested in a recent comment.[18] After describing the experimental setup, we thus start the main part of this paper by discussing the differences we observe in both ARPES and the low-energy-electron-diffraction (LEED) pattern for the different cleavage planes. The result of this discussion influences the way we analyze our data and the choice of the spectra we finally use in comparing our results with the bulk LDA calculations, two topics which are discussed in the subsequent chapters.

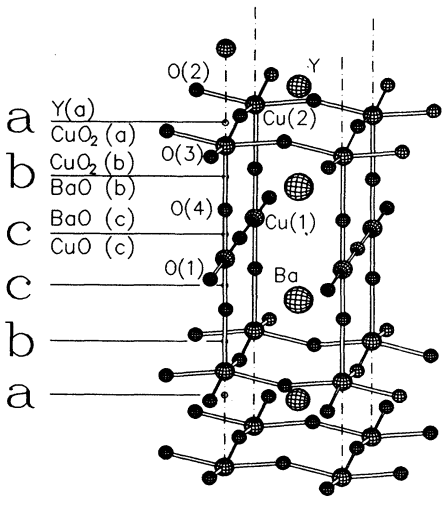

FIG. 1. The unit cell of Y-Ba-Cu-O. The letters *a*, *b*, and *c* refer to cleavages between the Y and the CuO layers, the CuO and the BaO layers, and the BaO and the CuO layers, with the upper and lower surface thus generated labeled accordingly.

II. EXPERIMENTAL

The facilities of the experimental setup are described in detail in Ref. 8. Hence we confine our description to the main points of interest. The $YBa_2Cu_3O_{7-\delta}$ $(0.1<\delta<0.2)$ single crystals were grown in an Al_2O_3 crucible by the slow cooling method, using a Cu-BaO self-flux.[19] After growth, the remaining melt was sucked up by a porous ZrO_2 ceramic, leading to nearly free-standing crystals. Oxidation of the extracted crystals was carried out in a pure O_2 atmosphere at 1 bar and various temperatures and times between 580 and 420 °C during 50 and 80 h. As a consequence of the crucible corrosion, the crystals contain some Al on the Cu(1) sites leading to an inductively measured T_c value of 86 K. Investigation by polarization microscopy revealed the presence of twins and a large orthorhombicity of the crystals. Their dimensions were about $4\times4\times0.8$ mm^3.

The Y-Ba-Cu-O samples were cleaved by guiding a razor blade exactly along a (001) plane towards the edge of the crystal. The cleavage was performed in ultrahigh vacuum (10^{-10} mbar) between 10 and 20 K and the samples were held at these temperatures during the measurements in order to prevent the possible loss of oxygen from the surface region. Due to the surface sensitivity of photoemission, this loss would severely affect the ARPES results.[20,21]

To check the quality and orientation of the cleavage planes we recorded some LEED patterns, but only after finishing the photoemission work, since the electron beam of the LEED gun might change the surface structure of the samples.[22] The pattern which shows sharp integral order spots remained unchanged for at least 30 h if the samples were held at low temperature. The surfaces, however, are not smooth on a macroscopic scale. Scanning electron micrographs taken at room temperature show that the cleaved surfaces consist of numerous terraces, with typical lateral dimensions of 0.1 mm. This surface roughness is also responsible for an unusually large amount of stray light.

Photons are provided by the 2 m Seya beamline at the Berliner Elektronenspeicherring für Synchrotronstrahlung (BESSY). The focus on the sample has a diameter of about 0.5 mm. The polarization vector of the incident light is oriented parallel to the plane of detection. This plane coincides with both the (100) and (010) crystal planes, since all of the samples are twinned. Electrons emitted from the surface are detected for eight different coplanar emission angles simultaneously. The analyzer consists of a high- and a low-pass filter together with a preretarding stage. The energy resolution is controlled by setting the energy separation of the two filters. The angular resolution of this instrument is 2° and the ultimate energy resolution 25 meV full width at half maximum (FWHM).

For optimal performance, we traded some energy resolution for a higher signal-to-noise ratio. The large amount of scattered light is the origin of a constant back-

ground signal, independent of the energy resolution of the analyzer. Since the signal-to-noise ratio at the highest energy resolution is dominated by this background signal, we set the combined energy resolution of both the 2 m Seya and the electron analyzer to values between 60 and 70 meV FWHM. These values are actually determined by fitting the measured Fermi edge of a polycrystalline Ag or Pt sample to the convolution of the Fermi-Dirac function with a Gaussian, treating its FWHM as a fit parameter.

III. SURFACE DEPENDENCE

In principle, the Y-Ba-Cu-O crystal could be cleaved perpendicular to the c axis (a) between the Y layer and the Cu(2)-O(2)O(3) planes, (b) between the Cu(2)-O(2)O(3) planes and the Ba-O(4) planes, and (c) between the Ba-O(4) planes and the Cu(1)-O(1) chains. Since each cleavage exposes different upper and lower surfaces, there is a total of six different basal planes which are shown in Fig. 1. Owing to the limited escape depth of the excited electrons, one would expect at least different intensities of the ARPES features for the different basal planes, but since drastic electronic and/or structural changes are likely to occur at some of these basal planes, more dramatic effects could occur in the spectra.

However, it is quite likely that some of the surfaces will show a pronounced atomic reconstruction. Consider, e.g., case (a), which would generate an upper surface Y(a) containing all of the Y atoms while the lower surface $CuO_2(a)$ contains no Y at all. Since the bonding between the two layers has a strong polar character in the bulk, the LDA calculations show large modifications in the electron occupancy just below the $CuO_2(a)$ surface, larger than for any other surface investigated.[17] Thus some kind of reconstruction is bound to occur for the cleavage (a). The most natural rearrangement is that the upper and the lower surface both contain the same number of Y atoms which, instead of being distributed at random, will have the tendency to form a Y $c(2\times2)$ superstructure,[18] corresponding to optimal charge compensation.[17] Guided by these considerations, we carefully analyzed the low-energy-electron-diffraction (LEED) patterns obtained at 10 to 20 K after finishing the ARPES investigations. In addition to the sharp {10} spots we found broad and weak {1/2 1/2} spots characteristic of a strongly disturbed $c(2\times2)$ structure for the surface designated "sample 1" while these {1/2 1/2} spots are missing or much weaker in all other surfaces which we investigated by LEED. The presence and absence of these {1/2 1/2} spots is demonstrated in Fig. 2 which gives the intensity profile along a straight line connecting the (10) and the (01) spots for a primary energy of 60 eV. Clearly, a broad maximum centered at the (1/2 1/2) position is seen for sample 1 as expected for the Y $c(2\times2)$ surface, while this maximum is absent in the 1 eV sample which is characteristic of most other surfaces we generated by cleaving so far.

The difference between sample 1 and samples exhibiting the 1-eV peak is also quite pronounced in ARPES. The characteristic peak at 1 eV, which was defined as a sign of surface quality by Tobin *et al.*[16] but identified as a surface state by Claessen *et al.*,[23] is well developed for surface 2 but reduced to an edge for sample 1 (left-hand side of Fig. 3). On the other hand, if a low intensity of the 1-eV peak together with a high intensity of the peak close to E_F is taken as an indication of an electronic structure representative of the bulk (additional evidence for this conjecture is given later), sample 1 wins since its peak near E_F, measured at a different angle for optimal intensity, is clearly much more pronounced compared to the corresponding structure of sample 2 (right-hand side of Fig. 3).

It is tempting to interpret the difference in the energy position of the edge close to E_F (right-hand part of Fig. 3) as being caused by the BCS-type modifications of the spectrum obtained from sample 1. However, in view of the strong differences between the two spectra around 1 eV, part of the deviation around E_F could also be caused by differences in the surface electronic structure already in the normal state. One might also wonder why the midpoint of this edge falls above E_F for sample 2. In this case, the transition is located right at the point where the band passes through E_F, i.e., the corresponding Lorentzian is severely truncated by the Fermi function. The convolution with the Gaussian then produces the edge as given in the right-hand part of Fig. 3.

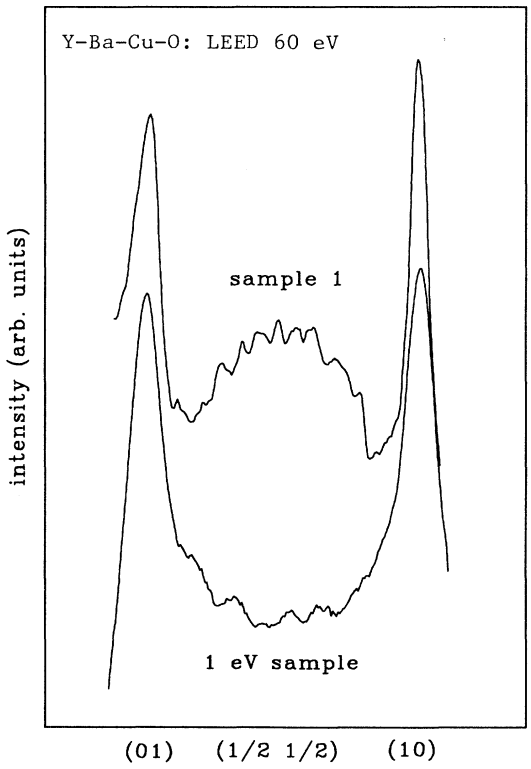

FIG. 2. Intensity profile of a 60 eV LEED pattern along a straight line connecting the (01) and the (10) spots for two different cleavage planes. The cleavage and the recording of the LEED pattern was performed at temperatures between 10 and 20 K.

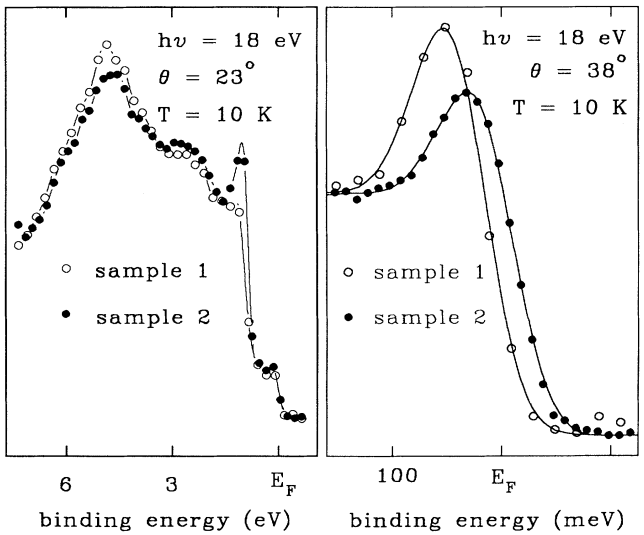

FIG. 3. The energy distribution function for two different surfaces. In the left-hand part, the angle of detection is selected to optimize the intensity of the 1-eV peak. The right-hand part shows the region close to the Fermi energy. Here, the angle of detection is selected for optimal intensity in this region.

In Fig. 4, both the lower (A) and upper (B) surface generated by one particular cleavage are investigated by an arrangement sketched in part (a). The numbers refer to the position of the light spot on the sample. The angle of observation is selected for high intensity of the 1-eV peak and the peak close to E_F in parts (b) and (c) of the figure, respectively. The two spectra taken at point 1 of the lower surface ($A1$) and at the corresponding mirror image of the upper surface ($B1$) agree much better than the two spectra taken at two different positions of the same surface ($A1$ and $A2$). This is true for both the 1-eV peak and the peak close to E_F. This experiment shows that the different terraces within the light spot expose both the upper and the lower surface even if only one particular bond is broken. For example, for cleavage (b), both $CuO_2(b)$ and $BaO(b)$ terraces must be present within the light spot since pronounced intensity differences between the spectra $A1$ and $B1$ should otherwise be present.

It is also possible that, e.g., terraces derived from both type (a) and (b) cleavages (see Fig. 1) are present within the light spot. Evidence for this is given in Fig. 5, which shows the spectra of 11 different cleavage planes, ordered according to decreasing intensity of the 1-eV peak. Again, the figure shows that the intensity of this peak depends drastically on the particular cleavage, but it also demonstrates that there is no simple correlation between its intensity and the variations of the structure at higher binding energy [part (a)] or the changes in intensity of the peak close to E_F. For example, the spectra of samples J and 1 both show only an edge at 1 eV but the peak close to E_F for sample 1 is much more pronounced than that of sample J. Sample 1 (its spectra are shown as open circles) seems to be unique since it is the only surface for which the 1 eV feature is reduced to an edge while simultaneously showing a narrow, high intensity peak at E_F and, as discussed above, a strongly disturbed $c(2\times2)$ superstructure of the surface.

As already reported by Claessen *et al.*,[23] we also find that even small amounts of adsorbed gases influence the 1-eV peak drastically. A definite decrease of its intensity with time is seen in Fig. 6(a), while no change of the peak near E_F occurs within about the same time interval [Fig. 6(b)]. Similarly, for sample 1 the peaks near E_F, shown for two angles of emission in Fig. 7, are perfectly reproduced after 24 h. The extreme sensitivity of the 1-eV peak to traces of reactive gases adsorbed on the surface, which is the standard test for a surface state, was recently investigated directly by Manzke *et al.*[24] An exposure of only 0.02 L H_2 corresponding to 0.02 monolayers reduces

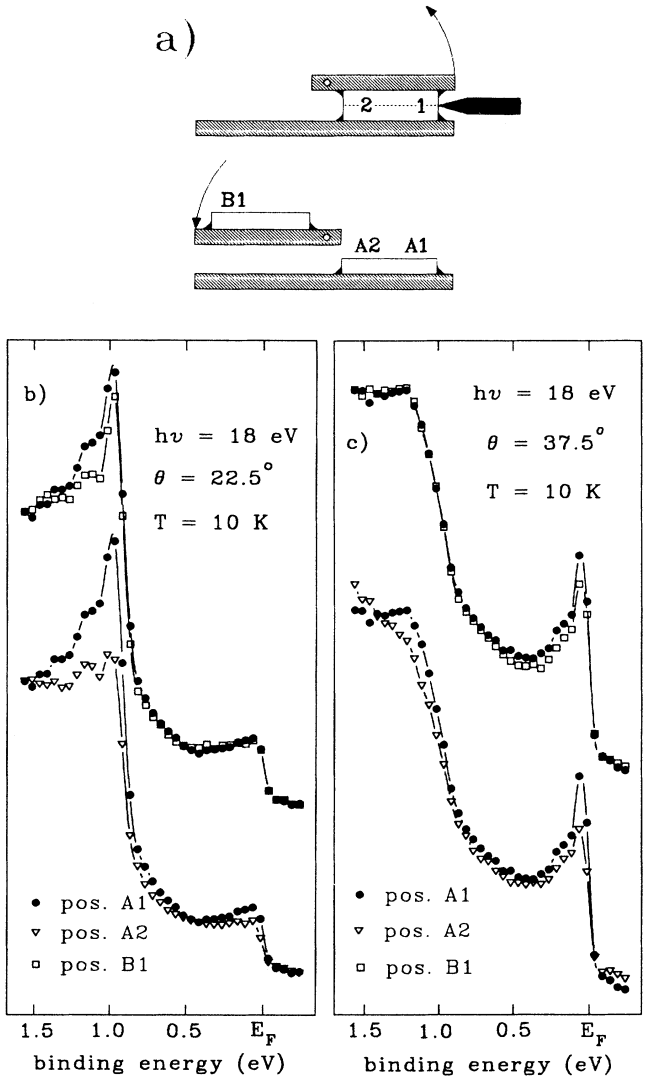

FIG. 4. Part (a) shows the cleaving arrangement. The numbers 1 and 2 refer to the position on the surface, the letters A and B to the lower and upper surface, respectively. In (b) and (c) the energy distribution curves are shown for two different angles of detection, optimizing the intensity at 1 eV and around 0 eV.

the peak height to 50% of its original value while after 0.5 L only a shoulder is left.[24] A similar test performed by Tobin *et al.*[16] did not show this sensitivity since the nonreactive Ar and O, which is already present in the crystal were used. Thus the experiments clearly establish the 1-eV peak as originating from a surface state.

Additional information about the nature of the 1-eV peak comes from the recent LDA investigations by Calandra *et al.*[17] of the different "ideal" basal planes of Y-Ba-Cu-O shown in Fig. 1, i.e., the bulk atomic positions were used and the possibility of compositionally "averaged" surfaces discussed above was not included. For fixed atomic positions, the authors calculate the local and the partial local density of states at the surface. Compared with the corresponding bulk quantities, they find pronounced changes for the cleavage (b) (see Fig. 1), leading to a nearly ideal stoichiometry at the BaO(b) plane which thus should be particularly stable, i.e., the cleavage (b) is likely to occur without reconstruction,

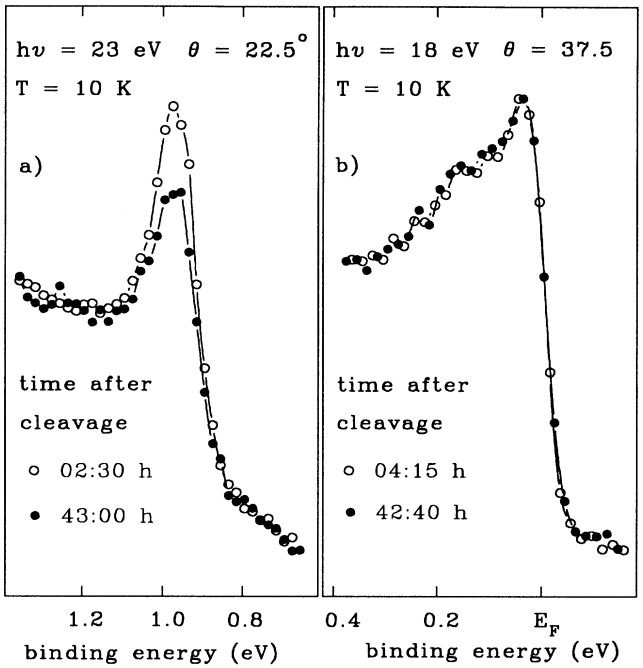

FIG. 6. The time dependence of the electron distribution curves of a surface showing a pronounced 1-eV peak. In (a) and (b) the angle of observation is selected for optimal intensity at 1 eV and around 0 eV, respectively.

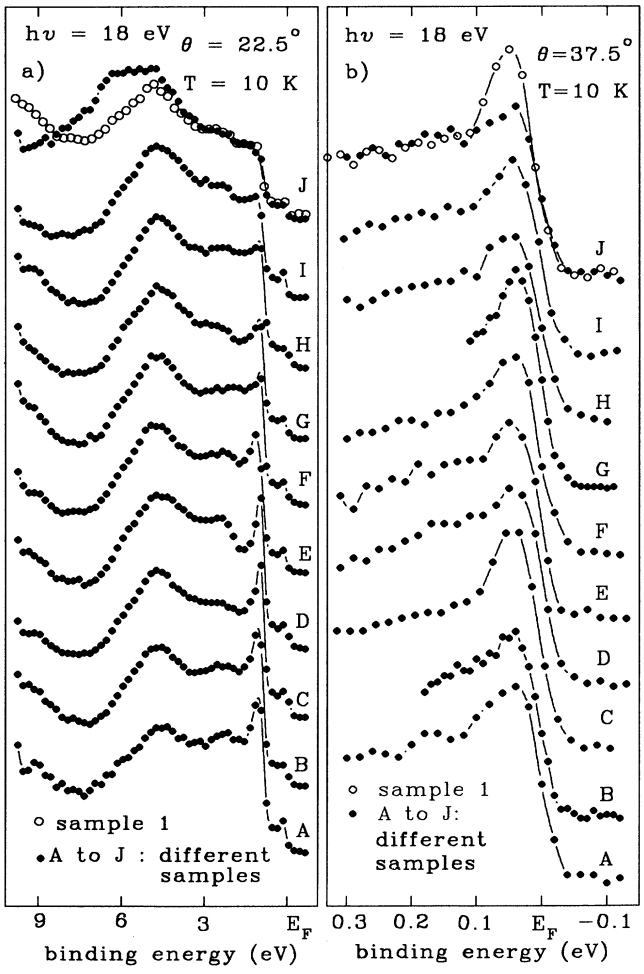

FIG. 5. The energy distribution curves for 11 different surfaces, ordered according to the intensity of the 1-eV peak. In (a) and (b) the angle of observation is selected for optimal intensity at 1 eV and around 0 eV, respectively. The spectra, shown as open circles, are taken at $T=20$ K and $\theta=38°$ in (b).

contrary to the behavior of cleavage (a) discussed above. The strong perturbation of the electronic structure by the (b) cleavage at and close to the BaO(b) and CuO_2(b) surfaces leads to the formation of prominent surface states at about 1 eV, which the authors identify with the corresponding peak in ARPES, and also at higher binding energies.

Calandra *et al.*[17] argue that cleavage (c) (see Fig. 1),

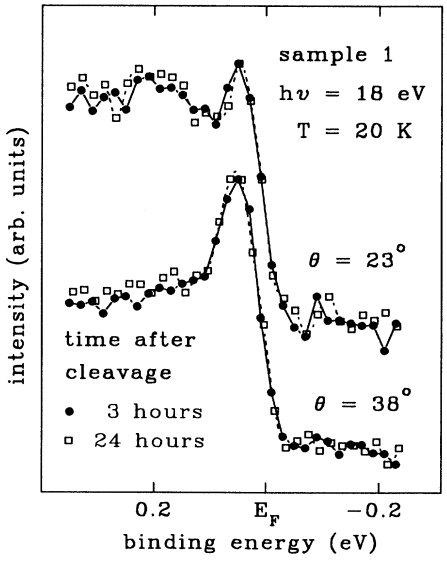

FIG. 7. The time dependence of the energy distribution curves for sample 1 at two different angles of detection.

which corresponds to cutting the Cu(1)—O(4) bond, is unlikely since it is stronger and has a shorter bond length in comparison with the Cu(2)—O(4) bond. Thus cleaving Y-Ba-Cu-O perpendicular to the c axis will probably result in a mixture of Y $c(2\times2)$, $CuO_2(b)$, and BaO(b) terraces, with the degree of mixing determined by the quality and the stoichiometry of the sample and possibly also by the cleaving procedure. Since the Y $c(2\times2)$ superstructure assures charge neutrality and no surface state has been found, ARPES taken at this surface might be more representative of bulk electronic properties in comparison with the corresponding spectra taken at the two (b)-type surfaces. In particular, since the building block sandwiched between the Y planes, known to be essential for the occurrence of superconductivity, is least affected by generating the Y $c(2\times2)$ surface, it might be even possible to find the BCS-type modifications of the spectra near E_F at low temperatures. On the other hand, the strong modifications of the electronic structure at and near the surface induced by creating either $CuO_2(b)$ or BaO(b), which cause the 1-eV surface state, are likely to destroy the superconductivity at the surface. We return to this topic in the following chapter.

IV. FIT PROCEDURE AND FERMI EDGE

Before starting a line-shape analysis it is imperative to remove the background inherent to each photoelectron spectrum. For a binding energy range of a few hundred meV around the Fermi edge, one has to consider mainly two contributions to the measured intensity. First of all there are always secondary electrons which have lost some of their energy due to inelastic scattering processes. The number of secondaries at a binding-energy E_b can be calculated approximately by assuming it to be proportional to the integration over the spectrum from E_b to E_F. Hence it seems reasonable to expect only a small number of them for energies near E_F. The second contribution is due to the finite width of the individual lines. To illustrate this effect, Fig. 8 shows a typical valence-band spectrum of Y-Ba-Cu-O (sample 1) together with the three constituting lines in the fit region between 0.6 and 7.9 eV and the corresponding total fit curve (thick line). The line corresponding to the peak at E_F was left out deliberately in order to demonstrate the contribution of the valence-band peaks to the measured intensity at the Fermi level. Note that the fitting of the valence structures was performed after stripping the spectrum of the secondary electrons by applying the procedure mentioned above. However, the effect of this treatment leaves the Fermi edge intensity nearly unchanged.

The lines shown in Fig. 8 are Lorentzian multiplied by the Fermi function and convoluted afterwards with a Gaussian to account for the experimental resolution, treating E_F as one of the fit parameters. An alternative procedure which led to the determination of the superconducting gap in the case of the Bi2:2:1:2 HTSC[9–12] is to use a BCS density-of-states function and to determine E_F separately from a metallic surface. We applied this method to more than 20 cleavage planes, which all showed the pronounced 1-eV surface-state peak, albeit

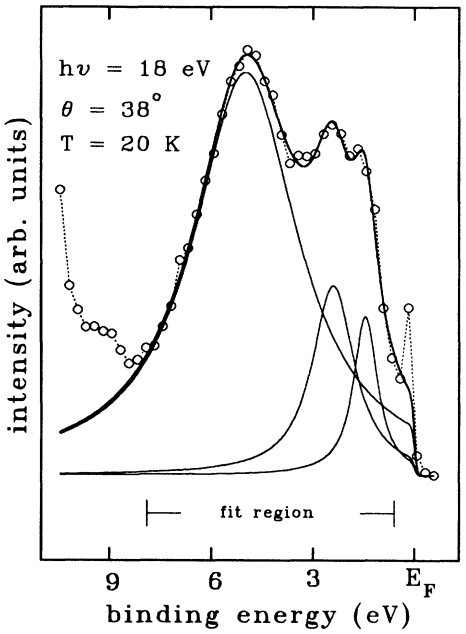

FIG. 8. Valence-band spectrum of sample 1 measured along Γ-$X(Y)$. The thick line is the total fit curve obtained as the sum of three Lorentzians. Note the high intensity at the Fermi edge, which is about 40% of the valence-band maximum, and the contribution of the lines in the fit region to this intensity.

with different intensities, determining E_F from the measured Fermi edge of a Pt surface at the same temperature as the Y-Ba-Cu-O surfaces (20 K), which is well below T_c. Within the experimental uncertainty of ±5 meV we obtain a zero BCS gap in all these cases, in perfect agreement with the results of two other investigations of spectra showing a prominent 1-eV peak[13,16] and also with the expectations discussed in the last chapter.

The surface of sample 1 does not produce the 1-eV surface-state peak, it is likely to be dominated by Y $c(2\times2)$ terraces, and it might thus be more representative of the bulk electronic structure at high *and* low temperatures. The results of the BCS analysis for spectra taken at $h\nu=18$ eV are shown in Fig. 9 (Ref. 18). For clarity, only the region close to E_F is given. The actual fit region, which is considerably broader, is 220 meV $> E_b > -120$ meV for the Ag sample and shown in Fig. 11 for sample 1. In the upper portion of Fig. 9, the open circles give the measured Fermi edge of Ag at 100 K. A technical defect at BESSY prevented us from measuring the Ag edge at 20 K directly after taking the sample 1 spectra. The solid line is the result of a least-squares-fit of the Fermi function at 100 K, convoluted with a Gaussian, to the measured Ag edge, treating E_F and the width of the Gaussian as fit parameters. The FWHM of the Gaussian turns out to be 70 meV, which we take as the combined energy resolution of our spectrometer. The dashed line is obtained by changing the temperature in the fit curve to 20 K without changing anything else; it deviates little from the corresponding 100 K fit. The dash-dotted line is the hypothetical BCS spectrum of a superconductor with $\Delta=20$ meV and a constant energy

distribution in the normal state, i.e., the BCS function convoluted with the Gaussian, using the FWHM and E_F as determined by the fit. As expected, the hypothetical BCS spectrum is shifted against the 20 K Fermi edge at low values of the energy distribution function and shows a pronounced overshoot at higher values, in spite of the attenuation of these features by the energy resolution of our spectrometer. Thus, given the high signal-to-noise ratio of our data, a gap of about 20 meV should be detectable. We also notice that the modifications between the 100 and 20 K Fermi edges are much smaller than between the Fermi edge and the hypothetical BCS curve.

The filled circles in the lower part of Fig. 9 are the data points of sample 1, taken at $T=20$ K and $\theta=40°$ six hours after the determination of the Ag edge. The solid line is the BCS least-squares fit to these points, using E_F and the FWHM of the Gaussian as determined from the Ag edge as input parameters but treating Δ as one of the fit parameters. Details of the procedure are described in conjunction with Fig. 11 below. The fit gives $\Delta=19$ meV, and similar fits to spectra taken subsequently at sample 1 within four hours at $\theta=25°$, 38°, 23°, and 35° yield $\Delta=20$, 22.5, 22, and 24 meV, respectively. The fit procedure thus yields reproducible results, except for a small drift of about 1 meV/h. It is also noteworthy that the spectra grouped at low and high θ values (typical examples are shown in the upper and lower part of Fig. 11), which correspond to transitions located in the first and second Brillouin zone, give the same Δ (disregarding the drift again). The main source of uncertainty in the Δ determination is of course a possible systematic error of E_F as determined from the fit to the Ag edge.

The fit procedure does not give the intensity ratio of the "sample 1" spectrum (solid line in the lower part of Fig. 9) to the Ag edge (dotted line in the lower and upper part), but since the "sample 1" spectrum should coincide with the hypothetical BCS spectrum (dashed-dotted line in the upper part) above E_F, we normalized it accordingly. Since a peak in the energy distribution function near E_F instead of a constant value is involved for the "sample 1" spectrum, the overshoot above the Ag edge below E_F is more pronounced than for the hypothetical BCS function.

Additional support for the gap value obtained from sample 1 comes from the analysis of the spectra shown in Fig. 10, which shows that we succeeded to obtain a pronounced Fermi edge also above T_c. This surface is different from sample 1 but it also does not show the 1-eV peak. The spectra were recorded at $h\nu=9$ eV. In performing the least-squares fit, we proceed again as described below for the spectra of Fig. 11, except for using only one Lorentzian in the fit region and the Fermi-Dirac and BCS function for 100 and 10 K, respectively. For the 10 K spectra, the best fit is obtained with the gap parameter $\Delta=24$ meV, which is close to Δ values obtained from

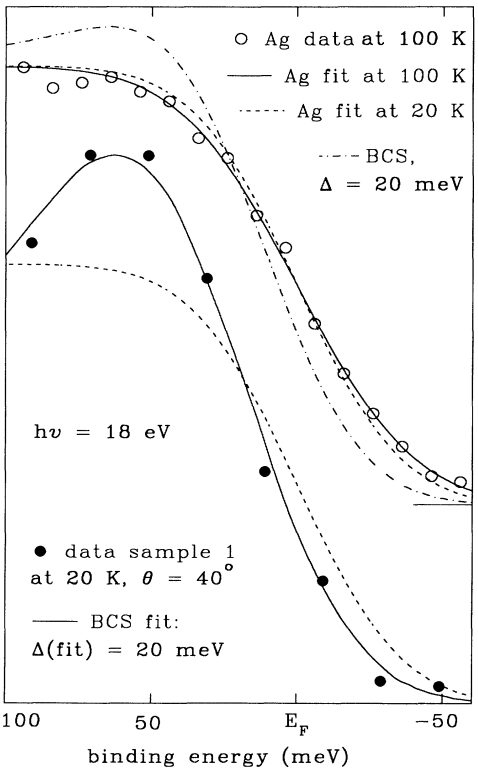

FIG. 9. The open circles give the measured energy distribution function of a polycrystalline Ag sample at 100 K, the heavy dots give the corresponding angle-resolved spectrum for sample 1 at 20 K. The solid lines are the corresponding fit curves obtained as explained in the text. The dashed line is the Ag edge transformed to 20 K, and the dash-dotted line is the spectrum of a hypothetical BCS superconductor with $\Delta=20$ meV.

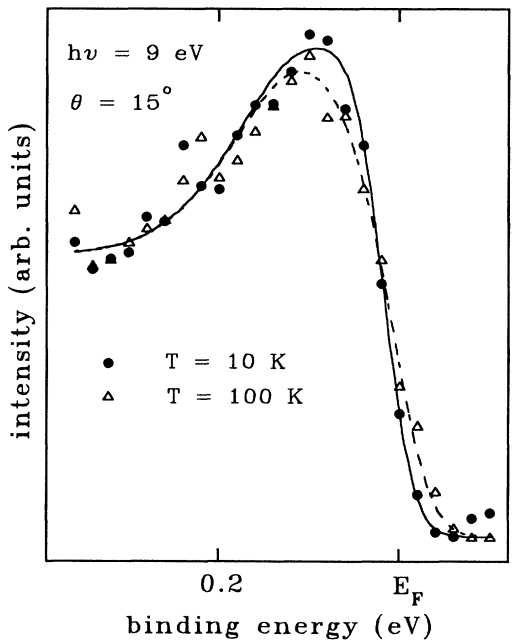

FIG. 10. Two ARPES taken at temperatures of 10 and 100 K. The solid and dashed lines result from a fit with a single Lorentzian line, multiplied by the Fermi-Dirac function (dashed line) and the BCS function with $\Delta=24$ meV (solid line), respectively, both convoluted with a Gaussian.

analyzing the five "sample 1" spectra (see Fig. 9). We emphasize that the two Δ values are obtained from two different samples at two different photon energies, even using two different 100 K references. The two spectra of Fig. 10 are normalized at the flat, high binding energy part of the curves, resulting in the characteristic differences close to E_F as described by the BCS theory which are again much larger than the temperature dependence caused by the Fermi function. In particular, the states missing at E_F are piled up at slightly higher E_b, as expected from the BCS theory. We emphasize that we do not consider the results derived from the spectra shown in Figs. 9 and 10 to be the final word on the subject, particularly since they were obtained at only two surfaces so far, but we do hope to stimulate more investigations of surfaces showing only a weak or missing 1-eV peak together with a pronounced peak at E_F and indications for the Y $c(2\times2)$ superstructure. As an example for the determination of the superconducting gap of Y-Ba-Cu-O by other methods we quote the infrared and Raman studies of the Stuttgart group (see Ref. 25 and the references quoted therein). Their analysis gives $2\Delta=316$ cm$^{-1}=39$ meV, in good agreement with our results.

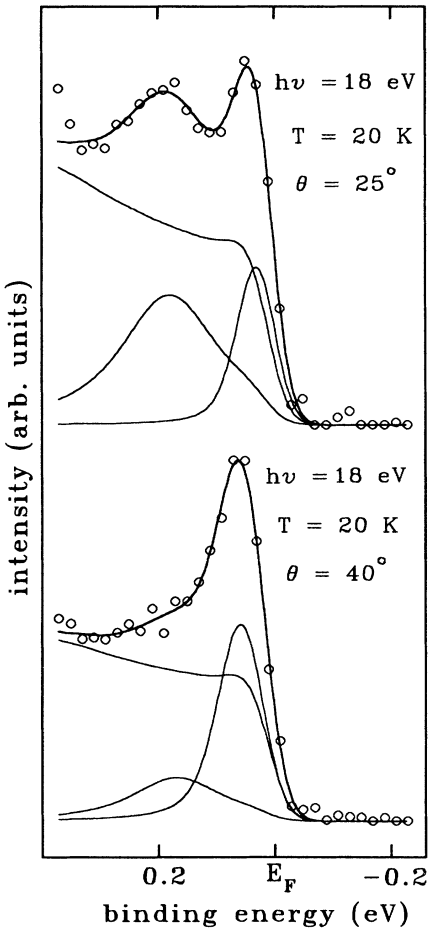

FIG. 11. Two ARPES of sample 1 together with the two contributing lines and the low-energy tail of states at higher binding energies. The heavy line corresponds to the total fit curve.

We now proceed to analyze the line shape of the $h\nu=18$ eV spectra within about 0.4 eV of E_F. The number of lines used for the fit and the treatment of the background can best be explained by referring to Fig. 11, which shows two very different spectra composed of two peaks within the fit region. As was explained above, most of the "background" in this range stems from the finite broadness of the lines at higher binding energies. It is well known that the valence structures show intensity variations and probably dispersion as well, depending on their position in k space and the orientation of the polarization vector of the incident radiation. Hence the steepness and intensity of the tails extending into the fit region is modified, too. We try to account for this by using one additional peak at higher binding energies and allow its height and position to vary during the least-squares fit. The lines used for this procedure are Lorentzians again, which were multiplied by the BCS function and convoluted with a Gaussian due to the instrumental broadening.

Special care has to be employed on how to model the increase of the peak width with increasing binding energy. This dependence is closely related to the issue whether or not the quasiparticles in the HTSC crystals form ordinary Fermi liquids. Generally the broadening is determined by the inverse lifetime of both photoelectrons and holes. If one considers a purely two-dimensional system only the lifetime of the holes contributes to the broadening.[26] Fermi-liquid theory predicts a quadratic increase of the inverse hole lifetime as $(E-E_F)^2$ with an infinitely sharp peak at the Fermi energy. However, a recent photoemission study of the Bi2:2:1:2 compounds revealed a linear dependence instead.[6] The situation for the Y-Ba-Cu-O system seems to be quite different. We tried to fit our spectra with both a quadratic and a linear ansatz and obtained comparable fit qualities for both models. It also turned out that peaks at E_F have finite widths, which means that a finite offset is needed in both cases. This seems to be an indication that also the final-state lifetime contributes to the broadening, i.e., the assumption of perfect two dimensionality for the initial states is not justified.

All the spectra shown in this paper were fitted using the formula $\gamma_L=a+b(E-E_F)^2$ for the Lorentzian linewidth, with the parameters $a=0.016$ eV and $b=2.16$ eV^{-1} as determined by preliminary studies. The fit parameters thus reduce to the energy position and intensity of the two lines within the fit region and that of the "background peak" at higher binding energies.

V. COMPARISON WITH BAND-STRUCTURE CALCULATIONS

In Fig. 12 we plotted eight selected ARPES taken at $h\nu=18$ eV and $T=20$ K for a variety of detection angles corresponding to the Γ-$X(Y)$ azimuth in k space. The solid lines are the total fit curves as obtained from the fit procedure described above. The spectra are arranged in such a way that the reduced value of k_t increases from the bottom to the top of the panel. The tangential component k_t is conserved in the emission of the photoelec-

tron and is determined by its kinetic energy and the polar angle in the usual way. Due to the large range of emission angles, most of the wave vectors k_t lie in the second BZ. The original location of k_t is marked by 1.BZ and 2.BZ, respectively.

As one can see from Fig. 12, a clear indication of band dispersion exists. While the dominating structure is centered at a binding energy of about 160 meV near the Γ point ($k_t^{\rm red}=0.05$ Å^{-1}), it shifts towards the Fermi level as the tangential component of the reduced wave vector $k_t^{\rm red}$ increases. For $k_t^{\rm red}$ between 0.64 Å^{-1} and the BZ boundary the peak is obviously cut off by the BCS density-of-states function. Simultaneously the broad structure at higher binding energy becomes most prominent in this region of k space. Note that the symmetrical line shape and the quadratic dependence which we chose to model the increase of linewidth with increasing E_g result in a good fit for all spectra. Furthermore, it is noteworthy that the intensities of the ARPES lines differ drastically between k_t values located in the first and the second BZ, respectively. The inset of Fig. 6 may serve as an example for this behavior. Shown is a spectrum of the same series of measurements, but with a much smaller emission angle corresponding to a value of $k_t=0.32$ Å^{-1} in the *first* BZ close to the two 0.30 and 0.34 Å^{-1} spectra with k_t in the *second* zone. The fact that drastic intensity variations can occur as a function of the extended k_t is well documented for such model systems like Cu[2,3] and could recently be observed for both the valence-band region of Bi2:2:1:2 (Ref. 8) and for states near E_F of Y-Ba-Cu-O.[13]

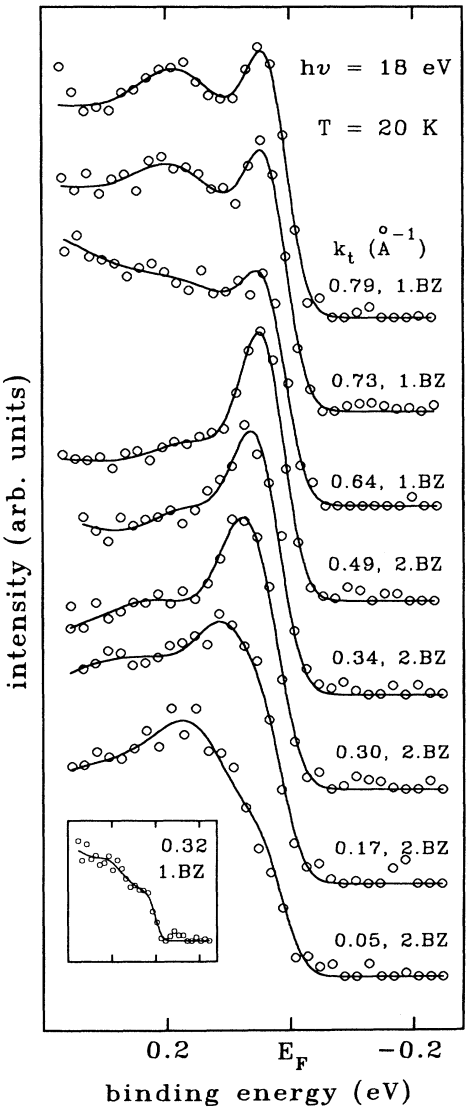

FIG. 12. Eight selected ARPES of sample 1 taken along the Γ-$X(Y)$ direction in k space. The solid lines are the total fit curves and the labels 2.BZ and 1.BZ are used to distinguish the values of k_t depending on their original location in the extended zone scheme. The inset shows a spectrum for $k_t=0.32$ Å^{-1} (1.BZ) and clearly demonstrates the k dependence of the dipole matrix element.

As we have noticed above, the dominating structure of the spectra is cut off by the BCS density-of-states function for $k_t^{\rm red}$ values in the range between 0.64 Å^{-1} and the BZ boundary ($k_t=0.82$ Å^{-1}). This is indicative of a band crossing or at least touching the Fermi surface in this region of the BZ. A comparison of these values with the recently published local-density-functional (LDF) calculation of the Fermi surface by Pickett *et al.*[27] is shown in Fig. 13. Plotted is the projection of the Fermi surface onto the basal plane ($k_n=0$ Å^{-1}) of the BZ for all values of the normal component k_n. The shaded regions denote those parts in the plane for which a Fermi surface exists for some values of k_n. It can be seen that the projected Fermi surface of the chain-derived band is well defined around the $\Gamma(Z)$ point while the broadening in the vicinity of $X(U)$ reflects a considerable amount of k_n dispersion. The points corresponding to our spectra (partly shown in Fig. 12) are plotted both along the $\Gamma(Z)$-$X(U)$

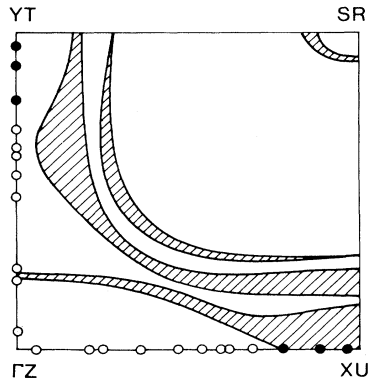

FIG. 13. Comparison of the calculated (Ref. 20) and experimentally determined Fermi surface. The projection of the Fermi surface onto the basal plane of the Brillouin zone for all values of k_n is symbolized by the shaded regions. The filled and open circles correspond to experimental points depending on whether or not the ARPES structures are cut off by the BCS density of states function. The points are plotted both along Γ-X and Γ-Y.

and $\Gamma(Z)$-$Y(T)$ directions and are symbolized by filled and open circles depending on whether or not the corresponding peak is cut off by the BCS function. While the projected Fermi surface around the $X(U)$ point is well reproduced by the experiment, there is no experimental evidence for the intersection of the chain-derived band with the Fermi surface along $\Gamma(Z)$-$Y(T)$.

Before starting a comparison of the experimentally derived $E(\mathbf{k})$ dependence with the calculated bands, it is helpful to discuss a second series of experiments first, since it sheds some light on the influence of crystal twinning and the intensity variations on the photoelectron spectra. These measurements were performed at $h\nu=9$ eV with the surface, which was also used to obtain the spectra shown in Fig. 10. Aside from the different photon energy all experimental conditions are the same as above. Figure 14 shows some selected spectra of this series for emission angles between 3° and 41° corresponding to k_t values between 0.06 and 0.7 Å^{-1}. Due to the lower photon energy all the k_t are located in the first BZ. Even accounting for the smaller signal-to-noise ratio of these spectra, it is obvious that they differ markedly from the ones given in Fig. 12 which is again a typical band-structure behavior. The twinning results in the superposition of transitions with k_t along Γ-X and Γ-Y, but the dispersion perpendicular to the surface also has to be considered. Even if k_t is the same, the normal components k_n and thus the binding energies of the initial states will vary for the two photon energies. Combined with the different final states, the transition probability and also the number of transitions contributing to the particular peak will show drastic variations for the two photon energies, explaining the observations at least in principle. While the superposition of the various components with different intensities combines to produce one apparent broad peak for $h\nu=9$ eV, two peaks are clearly resolved for $h\nu=18$ eV. We therefore restrict the quantitative analysis to the $h\nu=18$ eV spectra taken on sample 1.

We tackle the combined problems of twinning, unknown k_n, and drastic intensity variations by assuming the final states to be those of the free electron. This might be a reasonable approximation since the final energy is about 18 eV above E_F and since the small escape depth eliminates the band gaps which would be present at the BZ boundaries without damping.[3] In Fig. 15, the lines of constant initial and final energies and the BZ boundaries are shown schematically in the plane of observation. The two initial states are chosen to belong to the same star of $\mathbf{k}$, i.e., they are degenerate, although the photoelectrons excited from them are observed under different polar angles, as shown in the top part of the figure. Within the above approximation, the transition probability is

$$w=|\langle f|\,\mathbf{A}\cdot\mathbf{p}|i\rangle|^2=|C_m h/2\pi\mathbf{k}\cdot\mathbf{A}|^2\ ,$$

where C_m is the Fourier coefficient of the plane-wave component with $\mathbf{k}=\mathbf{k}^{\mathrm{red}}+\mathbf{G}_m$ in the initial state. Thus $w_1\neq w_2$ not only since $\mathbf{k}_1\cdot\mathbf{A}\neq\mathbf{k}_2\cdot\mathbf{A}$ but also since $m_1\neq m_2$. Thus, although $E(\mathbf{k})$ is periodic in reciprocal space, the intensity of the ARPES lines is not, a statement which is, of course, independent of our approximation.[28] Similarly, the volume of k space which is proportional to the number of states contributing to transitions 1 and 2 is also different. It is determined by the experimental resolution and the gradients of the initial and the final band; in our approximation the gradient of the final band is proportional to $\mathbf{k}$ and thus clearly different for the two transitions. The intensity variations within Fig. 12 and between Fig. 12 and Fig. 14 as discussed above, and similar variations noticed by other authors[13] are thus to be expected, they should be taken into account in

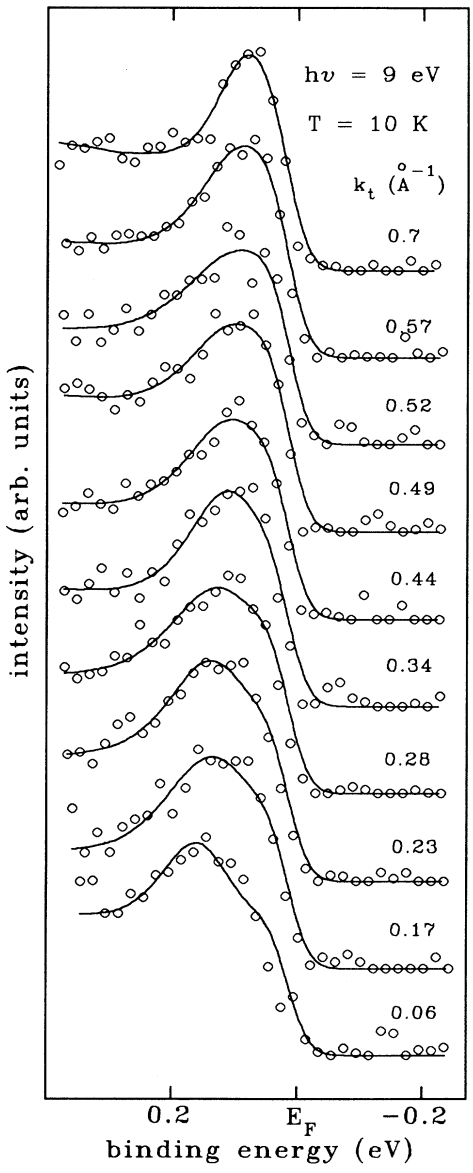

FIG. 14. Some observed ARPES measured along Γ-$X(Y)$ for varying values of k_t in the first BZ. The fit curves (solid lines) are obtained as before but using only one Lorentzian in the fit region. The surface is the same as that used to record the spectra of Fig. 10.

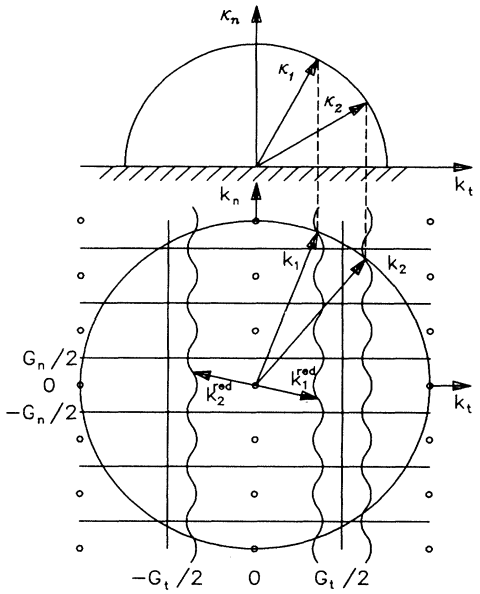

FIG. 15. Schematic representation of the lines of constant initial (wavy lines) and constant final energy in the bulk (large circle) and in vacuum (half circle) in the plane of observation, together with the BZ boundaries. Two transitions from two degenerate initial states belonging to the same star of **k** are shown; the corresponding photoelectrons are observed under different polar angles.

analyzing the ARPES results as we did in the case of the Bi2:2:1:2 spectra.[8]

We now give a quantitative analysis of our spectra, using the free-electron approximation for the final states. In order to do so, we must know the position of the free-electron parabola with respect to the calculated initial bands,[27] which are shown in Fig. 16. The four lines with different drawing patterns denote bands along Γ-X and Γ-Y in the basal plane and the corresponding bands along Z-U and Z-T at the top or bottom of the BZ, respectively. The points are the result of our line-shape analysis; we attach the highest confidence to the filled circles, the lowest to the open circles, with the dotted circles in between. Recalling the discussion of Fig. 13, we notice that the point close to E_F at $k_t^{red}=0.64$ Å^{-1} corresponds to the Z-U branch crossing E_F, i.e., k_n^{red} at the top of the BZ. We now adjust the inner potential V_0, which is the difference between the vacuum level and the minimum of the free-electron parabola of the final states in order to fulfill this requirement, taking the $h\nu=E_f-E_i=18$ eV into account. Possible solutions for V_0 are e.g., 22, 10.5, and 2 eV, with no other solutions in between. We settle for $V_0=10.5$ eV since this is closest to typical values needed for calculating the intensities of the diffraction spots produced by low-energy electrons. The k_n^{red} values calculated with $V_0=10.5$ eV are given at the top of Fig. 16; the values are actually the average of the two points corresponding to the two ARPES lines for each polar angle of observation, since the individual values differ by only about 2% of the BZ diameter in the direction of the surface normal which is $G_n=0.54$ Å^{-1}. The three underlined values of k_n^{red} correspond to k_t in the first BZ, the remaining values belong to k_t falling in the second BZ.

The three other points with $k_t^{red}>0.64$ Å^{-1} close to E_F have somewhat smaller k_n^{red} which is, however, still comparable to $G_n/2$. We thus would expect them to be still relatively close to the Z-U band if it were not for the intersection of this band with E_F which forces the remnants to peak at very low binding energies. Likewise we assign the corresponding four points at about 0.2 eV to the Z-T branch because they are close to it in energy and k_n^{red}. For k_t^{red} between 0.6 and 0.2 Å^{-1}, k_n^{red} abruptly drops to small values, i.e., close to the basal plane of the BZ. This drop is caused by k_t falling in the second BZ for all these points. We thus expect the experimental points to be close to the Γ-X and Γ-Y branches. This is indeed the case for Γ-X if we assign the two points at

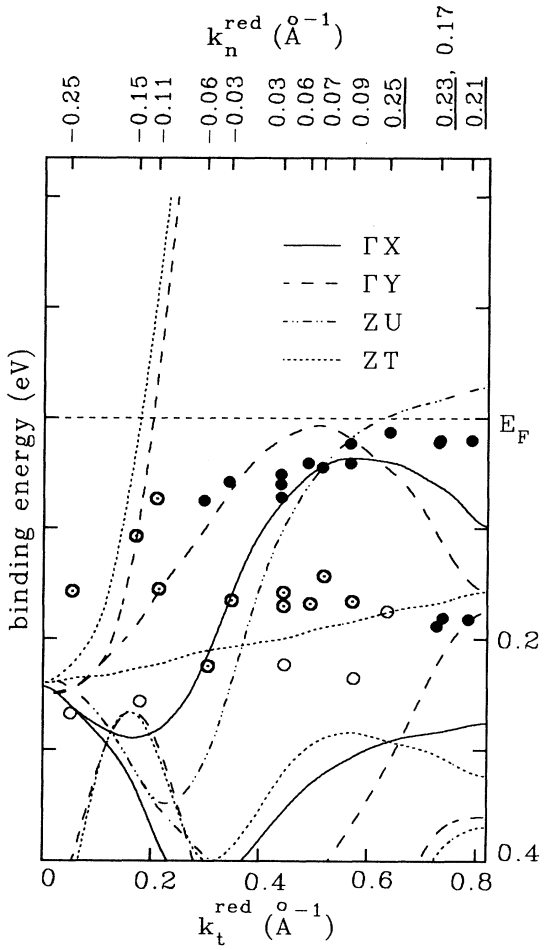

FIG. 16. Calculated bands along four high-symmetry directions of the Brillouin zone. The circles denote the experimentally determined $E(\mathbf{k})$ dependence as obtained from the least-squares-fit procedure for all the spectra of sample 1. The reliability of the points is indicated by their filling (full: high, dotted: medium, open: low). The k_n values at the top of the figure are obtained by assuming free-electron final states with an inner potential of 10.5 eV.

$E_b \simeq 0.2$ eV and $k_t^{\text{red}} \simeq 0.3$ Å^{-1} to this band and the corresponding points at about 0.06 eV to Γ-Y. This implies a crossover of the experimental points from Z-U to Γ-X at about the crossing of the calculated bands, which is clearly supported by the experiments. We expect a similar crossover of the points assigned to Z-T and Γ-Y, but since the corresponding calculated bands do not cross, they only predict the energy region of the expected crossing, again compatible with our assignment.

The three pairs of points below $k_t^{\text{red}} = 0.3$ Å^{-1} correspond to k_n^{red} values between the basal plane and the bottom of the BZ at -0.27 Å^{-1}, which makes an assignment more difficult. In addition, the increasing width of the peaks decreases the accuracy of the experimentally determined binding energy. The two points at about 0.1 eV and $k_t^{\text{red}} \simeq 0.2$ Å^{-1} might belong between the two steep Γ-Y and Z-T bands crossing E_F. The point at $k_t^{\text{red}} = 0.05$ Å^{-1} and 0.16 eV is near the bottom of the BZ and could thus be assigned to the steep Z-T band, for which the calculation gives 0.22 eV at this point of k space. This discrepancy might just be caused by the decreased experimental accuracy, but it might also hint at the narrowing of this band by strong electron correlations.

VI. SUMMARY

We find considerable variations in ARPES of Y-Ba-Cu-O for different cleavage planes perpendicular to the c axis, which are likely to be caused by a varying mixture of Y $c(2\times2)$, $CuO_2(b)$, and $BaO(b)$ terraces. The 1-eV surface state is characteristic of the strong modifications in the low- and high-temperature electronic structure at and near the $CuO_2(b)$ and the $BaO(b)$ surfaces. Occasionally, the cleaved surfaces show indications of the Y $c(2\times2)$ superstructure in LEED together with a pronounced Fermi edge but no 1-eV peak in ARPES. The electronic structure at these surfaces seems to be more representative of the bulk, and BCS-type modifications of the Fermi edge at low temperatures can be detected.

We have performed a line-shape analysis of ARPES, taken at low temperatures on two Y $c(2\times2)$dominated surfaces along the Γ-$X(Y)$ azimuth. The 18 eV spectra show a very sharp line close to E_F with a peak intensity of up to 40% of the valence-band maximum. Additionally, we could clearly resolve a second peak at a binding energy of about 200 meV. By comparison, only one broad peak can be discerned in the 9 eV spectra. The spectra show typical band-structure features, i.e., energy dispersion and strong intensity variations of the peaks with angle of observation and photon energy. The 100 K spectra show the Fermi edge expected for the metallic state.

Approximating the final state as that of the free electron, we can account qualitatively for the observed intensity variations. Furthermore, adjusting the inner potential to 10.5 eV and considering the twinning of the crystal, the $E(\mathbf{k})$ extracted from the 18 eV spectra agrees well with a recent LDA calculation. A quadratic increase of the ARPES linewidth with the binding energy is compatible with our results, indicating that the quasiparticles in Y-Ba-Cu-O form a normal Fermi liquid. This strong increase of the linewidth with the binding energy suggests, together with a possible narrowing of one experimentally determined band, that electron correlations are important in Y-Ba-Cu-O.

ACKNOWLEDGMENTS

We would like to thank the staff of Berliner Elektronenspeicherring-Gesellschaft für Synchrotronstrahlung (BESSY) for their professional work in general and for helping us out on many occasions in particular. In addition, we acknowledge the financial support by the Deutsche Forschungsgemeinschaft through the Sonderforschungsbereich 252 Darmstadt/Frankfurt/Mainz, and by the Bundesminister für Forschung und Technologie under Contract No. 05 346AA I8. Finally, we would like to thank M. Onellion for his criticism which induced some last minute changes in the description of our data analysis.

[1] P. W. Anderson and R. Schreiffer, Phys. Today **44**, 54 (June 1991).

[2] E. Dietz and U. Gerhardt, J. Phys. F **8**, 2213 (1978).

[3] E. Dietz and F. J. Himpsel, Solid State Commun. **30**, 235 (1979).

[4] C. J. Maetz, U. Gerhardt, E. Dietz, A. Ziegler, and R. J. Jelitto, Phys. Rev. Lett. **48**, 1686 (1982).

[5] A. Liebsch, Phys. Rev. Lett. **43**, 1431 (1979).

[6] C. G. Olson, R. Liu, D. W. Lynch, R. S. List, A. J. Arko, B. W. Veal, Y. C. Chang, P. Z. Jiang, and A. P. Paulikas, Phys. Rev. B **42**, 381 (1990).

[7] B. O. Wells, Z.-X. Shen, D. S. Desseau, W. E. Spicer, C. G. Olson, D. B. Mitzi, A. Kapitulnik, R. S. List, and A. Arko, Phys. Rev. Lett. **65**, 3056 (1990).

[8] R. Böttner, N. Schroeder, E. Dietz, U. Gerhardt, W. Assmus, and J. Kowalewski, Phys. Rev. B **41**, 8679 (1990).

[9] J.-M. Imer, F. Patthey, B. Dardel, W.-D. Schneider, Y. Baer, Y. Petroff, and A. Zettl, Phys. Rev. Lett. **62**, 336 (1989).

[10] Y. Chang, M. Tang, R. Zanoni, M. Onellion, R. Joynt, D. L. Huber, G. Margaritondo, P. A. Morris, W. A. Bonner, J. M. Tarascon, and N. G. Stoffel, Phys. Rev. B **39**, 4740 (1989); Y. Hwu, L. Lozzi, M. Marsi, S. La Rosa, M. Winokur, P. Davis, M. Onellion, H. Berger, F. Gozzo, F. Lévy, and G. Margaritondo, Phys. Rev. Lett. **67**, 2573 (1991).

[11] R. Manzke, T. Buslaps, R. Claessen, and J. Fink, Europhys. Lett. **9**, 477 (1989).

[12] C. G. Olson, R. Liu, D. W. Lynch, B. W. Veal, Y. C. Chang, P. Z. Jiang, J. Z. Liu, A. P. Paulikas, A. J. Arko, and R. S. List, Physica C **162-164**, 1697 (1989).

[13] G. Mante, R. Claessen, A. Huß, R. Manzke, M. Skibowski, Th. Wolf, M. Knupfer, and J. Fink, Phys. Rev. B **44**, 9500 (1991).

[14] J. C. Campuzano, G. Jennings, M. Faiz, L. Beaulaigue, B. W. Veal, J. Z. Liu, A. P. Paulikas, K. Vandervoort, H. Claus, R. S. List, A. J. Arko, and R. J. Bartlett, Phys. Rev. Lett. **64**, 2308 (1990).

[15]R. Liu, B. W. Veal, A. P. Paulikas, J. W. Downey, H. Shi, C. G. Olson, C. Gu, A. J. Arko, and J. J. Joyce, Phys. Rev. B **45**, 5614 (1992).

[16]J. G. Tobin, C. G. Olson, C. Gu, J. Z. Liu, F. R. Solal, M. J. Fluss, R. H. Howell, J. C. O'Brien, H. B. Radousky, and P. A. Sterne, Phys. Rev. B **45**, 5583 (1992).

[17]C. Calandra, F. Manghi, and T. Minerva, Phys. Rev. B **46**, 3600 (1992); C. Calandra, F. Manghi, T. Minerva, and G. Goldoni, Europhys. Lett. **8**, 791 (1989); C. Calandra and T. Minerva, Z. Phys. B **77**, 357 (1989).

[18]S. Ratz, N. Schroeder, R. Böttner, E. Dietz, U. Gerhardt, and Th. Wolf, Solid State Commun. **82**, 245 (1992).

[19]Th. Wolf, W. Goldacker, B. Obst, G. Roth, and R. Flükiger, J. Cryst. Growth **96**, 1010 (1989).

[20]R. S. List, A. J. Arko, Z. Fisk, S.-W. Cheong, S. D. Conradson, J. D. Thompson, C. B. Pierce, D. E. Peterson, R. J. Bartlett, N. D. Shinn, J. E. Schirber, B. W. Veal, A. P. Paulikas, and J. C. Campuzano, Phys. Rev. B **38**, 11 966 (1988).

[21]A. J. Arko, R. S. List, R. J. Bartlett, S.-W. Cheong, Z. Fisk, J. D. Thompson, C. G. Olson, A.-B. Yang, R. Liu, C. Gu, B. W. Veal, J. Z. Liu, A. P. Paulikas, K. Vandervoort, H. Claus, J. C. Campuzano, J. E. Schirber, and N. D. Shinn, Phys. Rev. B **40**, 2268 (1989).

[22]Y. Gao, T. J. Wagener, J. H. Weaver, A. J. Arko, B. Flandermeyer, and D. W. Capone II, Phys. Rev. B **36**, 3971 (1987).

[23]R. Claessen, G. Mante, A. Huss, R. Manzke, M. Skibowski, Th. Wolf, and J. Fink, Phys. Rev. B **44**, 2399 (1991).

[24]R. Manzke (unpublished).

[25]A. P. Litvinchuk, C. Thomsen, and M. Cardona, Solid State Commun. **80**, 257 (1991).

[26]T.-C. Chiang, J. A. Knapp, M. Aono, and D. E. Eastman, Phys. Rev. B **21**, 3513 (1980).

[27]W. E. Pickett, R. E. Cohen, and H. Krakauer, Phys. Rev. B **42**, 8764 (1990).

[28]E. Dietz and D. E. Eastman, Phys. Rev. Lett. **41**, 1674 (1978).